Novel Formulations of High-Performance Epoxy–Amine Networks Based on the Use of Nanoscale Phase-Separated Antiplasticizers

VALÉRIE SAUVANT, JEAN LOUIS HALARY

Laboratoire de Physicochimie Structurale et Macromoléculaire (UMR 7615), Ecole Supérieure de Physique et Chimie Industrielles de la Ville de Paris, 10, rue Vauquelin, F-75231 Paris cedex 05, France

ABSTRACT: The addition of an antiplasticizing agent in epoxy–amine resin formulations was revisited. The choice, as the antiplasticizer, of a chemical species which is fully miscible with the mixture of monomers but gives rise to nanoscale phase separation along the network construction was shown to be greatly favorable. Small domains, enriched in additive molecules, segregate in the polymer matrix, which is itself plasticized by residual additive molecules. Use of the additives did not change markedly the cure cycle and the total extent of reaction after full cure. The main effects of this special morphology on network properties were the depression of the glass transition temperature, T_g, of the matrix and the appearance of some damping (so-called μ-relaxation) in the temperature range intermediate between the secondary relaxation and the main mechanical relaxation. Networks prepared in this way were shown (1) to save a sufficiently high value of T_g in the view of the applications, (2) to present a higher modulus and higher toughness around room temperature than those of the conventional systems without an additive, and (3) to exhibit a lower water uptake at equilibrium than that of their regular homolog. © 2001 John Wiley & Sons, Inc. J Appl Polym Sci 82: 759–774, 2001

Key words: epoxy resins; antiplasticization; phase separation; fracture; water uptake

INTRODUCTION

Epoxy resins are a major class of thermosetting polymers, which are widely used as matrices for fiber-reinforced composite materials, adhesives, and coatings. Highly crosslinked epoxy networks, indeed, present a relatively high modulus, strength, and glass transition temperature. How-ever, these materials suffer from a lack of toughness, which is detrimental to many potential applications. Several methods have been proposed in an attempt to reduce brittleness by triggering energy-dissipating mechanisms inside the epoxy matrix. They have in common that they are based on the production of a two-phase morphology and they just differ by the nature and structure of the second phase, which may consist of rubbery domains, high-T_g thermoplastics, and stiff or core–shell particles. Unfortunately, the benefit in toughness obtained in this way was not decisive in the view of the applications, because of various penalizing counterparts such as the Young's modulus drop, complication of the network preparation process, and cost. Therefore, there remains a need for novel formulations of epoxy–amine res-
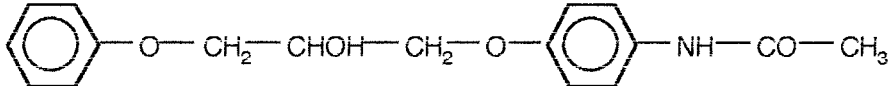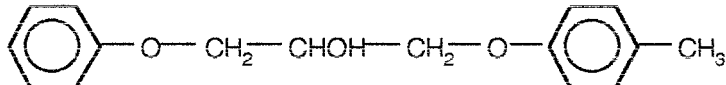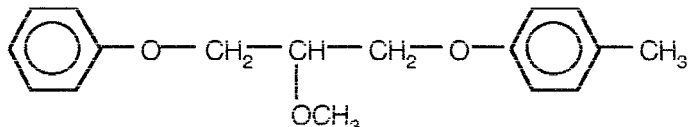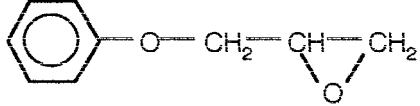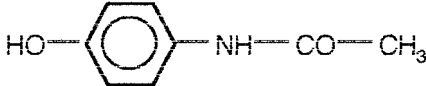
Table I   Formulas of the Additives and Additive Precursors Used in This Study

Chemical	Formula	Origin
Additive AA		Our lab
Additive AM		Our lab
Additive AO		Our lab
1,2-Epoxy-3-phenoxypropane (EPP)		Acros Organics
p-Hydroxyacetanilide (HAA)		Acros Organics
p-Cresol		Acros Organics

ins, intended to provide network toughness enhancement without significant impairment of other properties or processing conditions.

The starting point of our study was the consideration of the epoxy network antiplasticization by small-molecule additives, a phenomenon evidenced for a long time by Daly et al.[1] and recently understood on molecular bases.[2,3] Let us recall, for the sake of comprehension, the main results reported for the system diglycidyl ether of bisphenol-A (DGEBA)–hexamethylenediamine (HMDA)–aromatic acetamide (so-called additive AA in Table I). In the case of monomer mixtures fully cured in the presence of appropriate amounts of AA, dynamic mechanical measurements revealed a dramatic reduction in amplitude and width of the loss modulus peak associated with the secondary relaxation. In turn, decrease of the storage modulus is less pronounced in the modified network than in its regular homologs while passing the β-relaxation region. Finally, the room-temperature Young's modulus is fortified by the presence of the additive. The physical origin of the antiplasticization was shown to be the immobili-

zation of the network crosslinks by the additive molecules. As a result, those of the β-relaxation motions, which exhibit a cooperative character, are hindered. These cooperative motions occur on a larger spatial scale and exhibit a higher activation energy than do the isolated ones, which means that they are observed in the upper part of the broad β-relaxation damping peak of the network without an additive.

Suppose now that we replace the additive AA in the resin formulation by other antiplasticizers of lower compatibility toward the polymer chains under construction. Then, it may be expected that some phase separation occurs along the cure process and, in turn, improves the toughness of the materials. As a very simple idea, the increase in toughness should not be balanced by a decrease of the overall modulus, according to this scenario. Indeed, the decrease of the modulus accompanying the presence of the small molecule-enriched phase can be matched by the increase in the modulus associated with the antiplasticization.

To check the suitability of this strategy, diaminodiphenylmethane (DDM) and diaminodiphenyl

Table II   Epoxide and Amines Used in Network Preparation

Chemical	Formula	Origin
Diglycidyl ether of bisphenol-A (DGEBA)		Bakelite (Duisburg, Germany) (Rutapox 162)
Diaminodiphenylmethane (DDM)		Acros Organics (Geel, Belgium)
Diaminodiphenyl sulfone (DDS)		Ciba-Geigy (Basel, Switzerland) (HT976-1)

sulfone (DDS) (Table II) were chosen as the curing agent (instead of HMDA) to obtain networks with sufficiently high T_g's in the view of the applications. Also, two additives, so-called AM and AO (Table I), were synthesized and incorporated into stoichiometric mixtures of DGEBA–DDM and DGEBA–DDS. Calculation of the solubility parameters[4] was used as a rough but useful tool for selecting these additives. Values of the solubility parameters of interest, namely, δ_{ad} for AA, AM, and AO and δ_m for the repeat units of the resins, are given in Table III. Any increase in ($\delta_m - \delta_{ad}$) denotes a decrease of compatibility between the species, which will be continuously amplified along the polymerization of monomers as the result of unfavorable entropic contributions. In this respect, the additive AA should be very compatible with the monomer mixtures and remain miscible to the polymer networks, as actually reported.[5] On the other hand, the additive

AM, in which formula the polar amide moiety has been suppressed, presents a lower value of δ_{ad} and is likely to segregate from the network. This effect is reinforced in the case of the additive AO, of lower and lower δ_{ad}, for which hydrogen bonding to the epoxy chains is no longer likely to occur. The objective of the present article was to report on

1. The synthesis of the new additives AM and AO and of the modified networks;
2. The viscoelastic response of the networks, looking at the α-relaxation (depression of the glass transition temperature), the β-relaxation (antiplasticizing character of the additives), and the so-called μ-relaxation (associated with the additive-enriched phase);
3. The fracture behavior of the networks, to determine the critical stress intensity factor, K_{Ic}, and the critical energy release rate, G_{Ic}, as toughness indexes; and
4. The moisture uptake of the networks at equilibrium.

For sake of comparison, data relative to the networks without an additive and to those prepared in the presence of AA will also be given and discussed. Other aspects of the study[5] will be the matter of separate publications. They include evidence for phase separation by solid-state ^{1}H-NMR measurements,[6] the kinetics of the early stages of network construction, and some dielectric measurements.

Table III   Values of the Solubility Parameters Used to Predict the Compatibility Between Additives and Epoxy Networks

Chemical	δ_{ad} (MPa$^{1/2}$)	δ_m (MPa$^{1/2}$)
AA	26.5	
AM	24.0	
AO	20.8	
DGEBA–DDM		26.5
DGEBA–DDS		27.7

EXPERIMENTAL

Chemicals

The formulas and origin of the chemicals used in this study are given in Table I for the additives and additive precursors and in Table II for the regular components of the epoxy resins, namely, the diepoxide DGEBA and the diamines DDM and DDS. The antiplasticizer AA was prepared by following the procedure described by Daly et al.[1]: 1,2-Epoxy-3-phenoxypropane (EPP) and *p*-hydroxyacetanilide (HAA) at a 1.05 : 1 molar ratio were mixed and then heated at 150°C for 1 h in the presence of 0.1 wt % of diethylamine hydrochloride (Acros Organics, Geel, Belgium) as the catalyst. The reaction was roughly quantitative and AA, obtained in the form of a yellow amorphous material, was used without further purification. The additive AM was synthesized by following a similar procedure, based on the condensation of EPP onto *p*-cresol in the presence of diethylamine hydrochloride. The reaction material was purified by distillation under a vacuum. The third additive, so-called AO, resulted from the methylation of the alcohol function present in AM. To this end, methyl iodide (4 equiv) and AM (1 equiv) were mixed in toluene for 3 h at room temperature in the presence of silver oxide (2 equiv) and then the mixture was gently refluxed for 16 h. The mixture was filtered and then purified by distillation under a vacuum. Yield of the

Table IV   Code Names and Compositions of the Systems Under Study

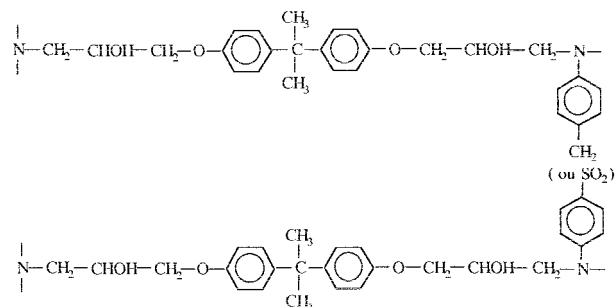| Code Name	Additive Weight Fraction, w_{add}
A–M	0
A–M–AA/29	0.09
A–M–AA/62	0.175
A–M–AA/96	0.247
A–M–AM/29	0.08
A–M–AM/62	0.154
A–M–AM/96	0.220
A–M–AO/62	0.161
A–M–AO/96	0.229
A–S	0
A–S–AA/29	0.087
A–S–AA/62	0.167
A–S–AA/96	0.237
A–S–AM/62	0.147
A–S–AM/96	0.211
A–S–AO/62	0.154

Figure 1   Repeat unit of the networks under study.

etherification reaction was checked by ^{1}H- and ^{13}C-NMR. AO showed a purity of 90%, the rest consisting of unreacted AM.

Synthesis of Epoxy Resins

The crosslinked epoxy resins were prepared from a stoichiometric mixture based on 2 mol of DGEBA and 1 mol of primary diamine (DDM or DDS). The modified formulations additionally included different amounts of additive per network unit (namely, 0.29, 0.62, and 0.96 mol per 4 hydroxypropylether units). The code names and compositions of the different samples under study are listed in Table IV. The network repeat unit is sketched in Figure 1.

To reach an epoxide–amine reaction as complete as possible, all the samples were submitted to adapted cure cycles. The resins based on DDM were cured at 80°C for 12 h and then postcured for 24 h at $\approx T_g + 30$°C (200°C for pure A–M, 160°C for the systems A–M–additive). No side reactions were detected during cure and postcure at the sensitivity of the NMR experiments. It was also checked that the number of unreacted epoxide groups, as controlled by FTIR after postcure, was actually very low. A difficulty was encountered in defining the cure cycle of the DDS-based resins, which should produce the higher cure extent in the absence of side reactions. On the one hand, DDS is less reactive than is DDM,[7] and, on the other hand, the networks A–S are sensitive to high-temperature degradation, as revealed by the marked decrease of T_g observed in the case of severe postcure.[8] As a compromise, DDS resins were first cured at 150°C for 6 h and then postcured for 3 h at 200°C in the case of pure A–S and at 160°C in the case of the systems A–S-additive.

Thermal Analysis

Glass transition temperature measurements were performed on the additives AA, AM, and AO

and on the cured resins by using a DuPont differential scanning calorimeter (DSC) 1090, operated at a heating rate of 10°C/mn. T_g was conventionally taken at the onset of the DSC traces. Before characterization, the samples (about 10 mg) were first heated above their T_g and then quenched with liquid nitrogen down to -150°C.

Specific heat-capacity measurements around the T_g were performed using a TA Instruments DSC 2920 equipped with a modulation option. Samples weighing between 3 and 10 mg were subjected to the following thermal history: (a) The encapsulated samples were initially heated in the DSC module up to a temperature T_0, significantly above their T_g (200°C for DGEBA–DDM, 100°C for pure additives) for 5 min to erase any previous thermal history; (b) then, the samples were quenched at a cooling rate of 10°C/mn from T_0 to $T_1 = T_g - 50$°C; and (c) the samples were finally scanned under a nitrogen atmosphere (50 mL/min) from T_1 to T_0 at an average heating rate of 5°C/min, modulated by a sinusoidal heating rate of ±0.8°C/min each 60 s.

Dynamic Mechanical Analysis

Viscoelastic experiments were performed on two different machines that gave useful data in previous studies.[2,9] A servohydraulic testing machine MTS 831, operated in the tensile mode and monitored by the software TestStar II, was used over the temperature range $-100/220$°C and the frequency range 0.02/60 Hz. A sinusoidal deformation of $\pm0.05\%$ was superimposed on a static deformation of about 0.1%. Measurements were performed on samples of size $4 \times 12 \times 52$ mm^3 and yielded, directly, the storage modulus, E', and the loss modulus, E''. A dynamic mechanical analyzer (DMA) DuPont DMA 983, operated in the flexural mode, was used to cover the low-temperature range ($-150/25$°C) at the frequency of 1 Hz. Samples of about $2 \times 10 \times 40$ mm^3 were submitted to a strain of 0.15%. The flexural data were transformed into E' and E'' by using a routine available on the DMA.

The characteristic temperatures of the mechanical relaxations were conventionally taken at the maximum of E'' at the frequency 1 Hz. In the secondary relaxation range, master curves were built according to shifts, a_{T/T_0}, along the reciprocal temperature axis. The activation energy, E_a, was calculated by assuming an Arrhenius dependence of the shift factors:

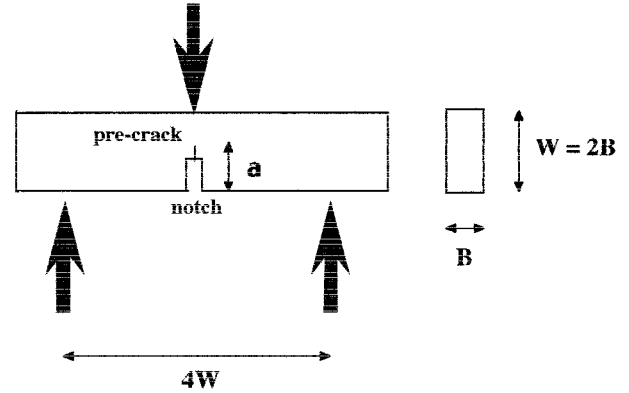$$\ln a_{T/T_0} = \frac{E_a}{R}\left(\frac{1}{T} - \frac{1}{T_0}\right) \tag{1}$$

Figure 2 Schematic drawing of a sample for the fracture test (the dimensions a, W, and B appear in eqs. (3)–(7)).

The activation enthalpy, $\Delta H^{\ddagger}$, and the activation entropy, $\Delta S^{\ddagger}$, were calculated using the relationships proposed by Starkweather[10]:

$$\Delta H^{\ddagger} = E_a - RT_0 \quad \text{and}$$
$$\Delta S^{\ddagger} = E_a - RT_0[1 + \ln(kT_0/2\pi h)] \tag{2}$$

where R, k, and h are the gas constant, Boltzmann's constant, and Planck's constant, respectively, and T_0 is the reference temperature.

Fracture

Plane-strain fracture tests were performed on three-point bending specimens (mode I), according to Williams protocol[11] (Fig. 2). A sharp pre-crack was formed with a fresh razor blade at the base of a machined notch. The specimens were then loaded in an MTS 810 testing machine at temperatures ranging from -20 to 60°C and at a constant crosshead speed of 1 mm/min.

The critical stress intensity factor for the initiation of crack growth, K_{Ic}, was calculated from

$$K_{Ic} = f\frac{P_{max}}{BW^{1/2}} \tag{3}$$

where B and W represent sample thickness and height, respectively, P_{max} is the maximum load recorded during the test, and f is a geometrical factor, corresponding to

$$f = 6\left(\frac{a}{W}\right)^{1/2} \frac{\left[1.99 - \frac{a}{W}\left(1 - \frac{a}{W}\right) \times \left(2.15 - 3.93\frac{a}{W} + 2.7\left(\frac{a}{W}\right)^2\right)\right]}{\left(1 + 2\frac{a}{W}\right)\left(1 - \frac{a}{W}\right)^{3/2}} \tag{4}$$

where a is the cumulated length of the notch plus precrack.

The critical energy release rate, G_{Ic}, was also determined experimentally by using the relation

$$G_{Ic} = \frac{U_i}{BW\Phi} \tag{5}$$

where U_i is the under curve area until load the reaches P_{max} and Φ is a geometrical factor equal to

$$\Phi = \frac{\Theta + 18.64}{\dfrac{d\Theta}{d\left(\dfrac{a}{W}\right)}} \tag{6}$$

Θ, appearing in eq. (6), should be calculated using the equation

$$\Theta = \frac{16\left(\dfrac{a}{W}\right)^2}{\left[1 - \left(\dfrac{a}{W}\right)\right]^2}\left[8.9 - 33.717\,\frac{a}{W} + 79.616\left(\frac{a}{W}\right)^2\right.$$

$$\left. - 112.952\left(\frac{a}{W}\right)^3 + 84.815\left(\frac{a}{W}\right)^4 - 25.672\left(\frac{a}{W}\right)^5\right] \tag{7}$$

For the experiments reported in the present article, the geometrical characteristics appearing in Figure 2 were set as $B = 6$ mm and $0.45 < a/W < 0.55$.

Moisture Uptake at Equilibrium

To reach the anhydrous state, the samples were dried for 48 h under a vacuum, at a temperature equal to $T_g + 30°C$. Pieces of the anhydrous samples, of mass m_{anh} and thickness e ranging from 0.8 to 4 mm, were placed for 2 weeks in a water-saturated atmosphere at 100°C. Weighing at regular intervals allowed one to determine the water percentage in the samples, $w(t)$, from the equation

$$w(t) = 100\,\frac{m_{wet}(t) - m_{anh}}{m_{anh}} \tag{8}$$

in which $m_{wet}(t)$ represents the mass of the sample at time t. It was checked that, at a sufficiently long time, $w(t)$ attains a constant value, w_∞, which does not depend on the sample thickness.

Therefore, one can consider that there is no gradient of water concentration after 2 weeks between the surface and the core of the samples. As a consequence, w_∞ is actually representative of the hydration of the materials at equilibrium.

In addition, the water-diffusion coefficient, D, could be calculated, in the approximation of a Fickian behavior, from the initial slope of the plots of $w(t)/w_\infty$ versus t/e, according to the equation

$$\frac{w(t)}{w_\infty} = \frac{4}{e}\,\sqrt{\frac{Dt}{\pi}} \tag{9}$$

In a simpler way, which has been used in the present article, D was derived from the value of t, so-called $t_{1/2}$, for which $w = w_\infty/2$, by means of the equation[12]

$$\frac{0.0494}{D} = \left[\frac{t}{e^2}\right]_{w(t)=w_\infty/2} \tag{10}$$

RESULTS AND DISCUSSION

Relaxation Behavior

General Features

Figure 3 presents plots of E'' as a function of temperature relative to the pure resin A–M and to the resins A–M containing 0.62 mol of the additive per network unit. The plot relative to pure A–M shows two mechanically active relaxations, namely, the α-relaxation at high temperature, in the glass transition region, and the broad β-relaxation, which develops mostly below ambient temperature. The sample A–M–AA/62 exhibits also the two relaxations α and β. The presence of the additive AA in the resin DGEBA–DDM is shown to affect the relaxations in a similar fashion as previously reported for the resins DGEBA–HMDA.[2] Indeed, plasticization effects occur in the glass transition region, as evidenced by the substantial depression of $T\alpha$. In addition, antiplasticization effects affect the secondary relaxation region, as revealed by the dramatic lowering of the E'' peak and a limited drop in the storage modulus E' while passing the relaxation. Interestingly, inspection of the main relaxation and secondary relaxation relative to the samples A–M–AM/62 and A–M–AO/62 reveals the same trends. Moreover, the samples A–M–AM/62 and A–M–AO/62 present an additional damping peak,
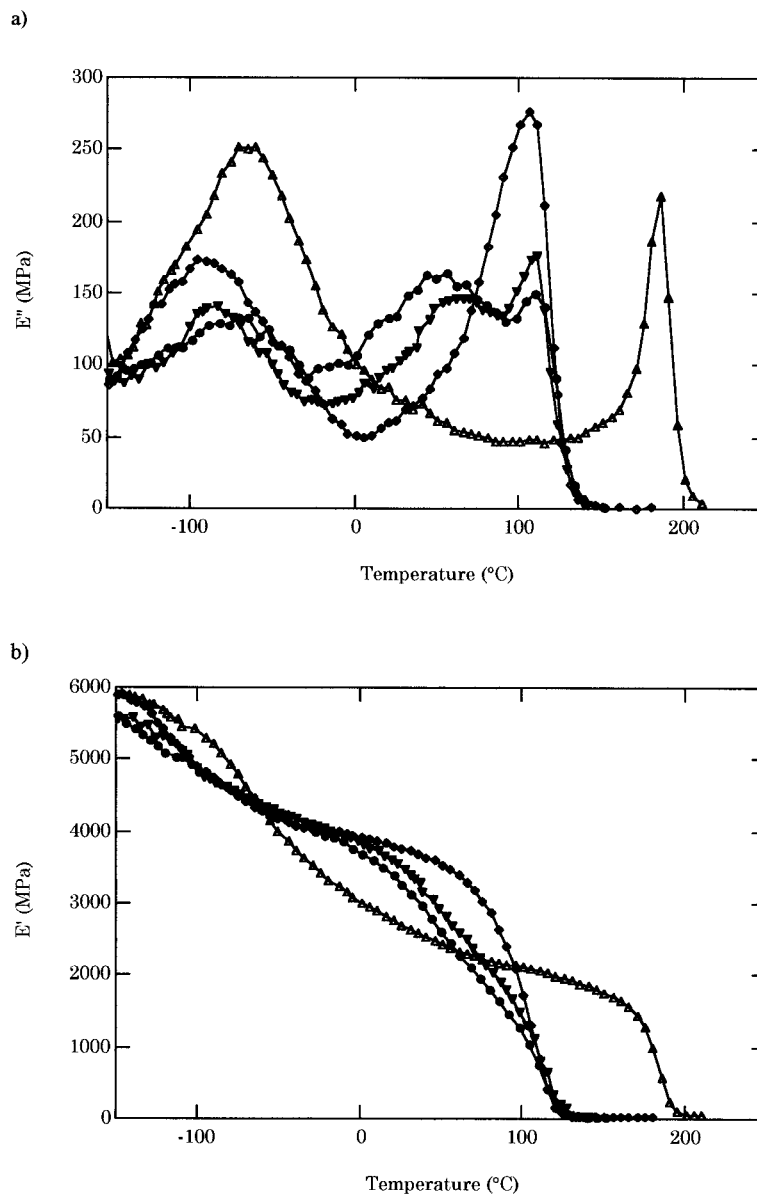
a)

b)

Figure 3 Temperature dependence of the loss and storage moduli at 1 Hz for the samples (△) A–M, (◇) A–M–AA/62, (▼) A–M–AM/62, and (●) A–M–AO/62: (plot a) loss modulus; (plot b) storage modulus.

relative to the so-called μ-relaxation, which develops between the relaxations α and β. This observation anticipates some segregation of the additives within the network.

All the above observations are true whatever the amounts of the additive in the range under study. They also remain valid irrespective of the nature of the resin, as illustrated in Figure 4 by data relative to the A–S series. The purpose of the next paragraphs was to investigate in more detail the main characteristics of the relaxations α, β, and μ.

Analysis of the β-Relaxation

The antiplasticizing character of the additive AA toward the relaxation of the networks DGEBA–DDM and DGEBA–DDS can be simply analyzed by analogy to our previous studies on the system DGEBA–HMDA–additive.[2,3] Indeed, the viscoelastic E'' traces [Figs. 3(a) and 4(a)] exhibit the same characteristics, showing that the high-temperature part of the relaxation disappears, while its low-temperature part remains about unchanged. For yet unexplained reasons, inspection,
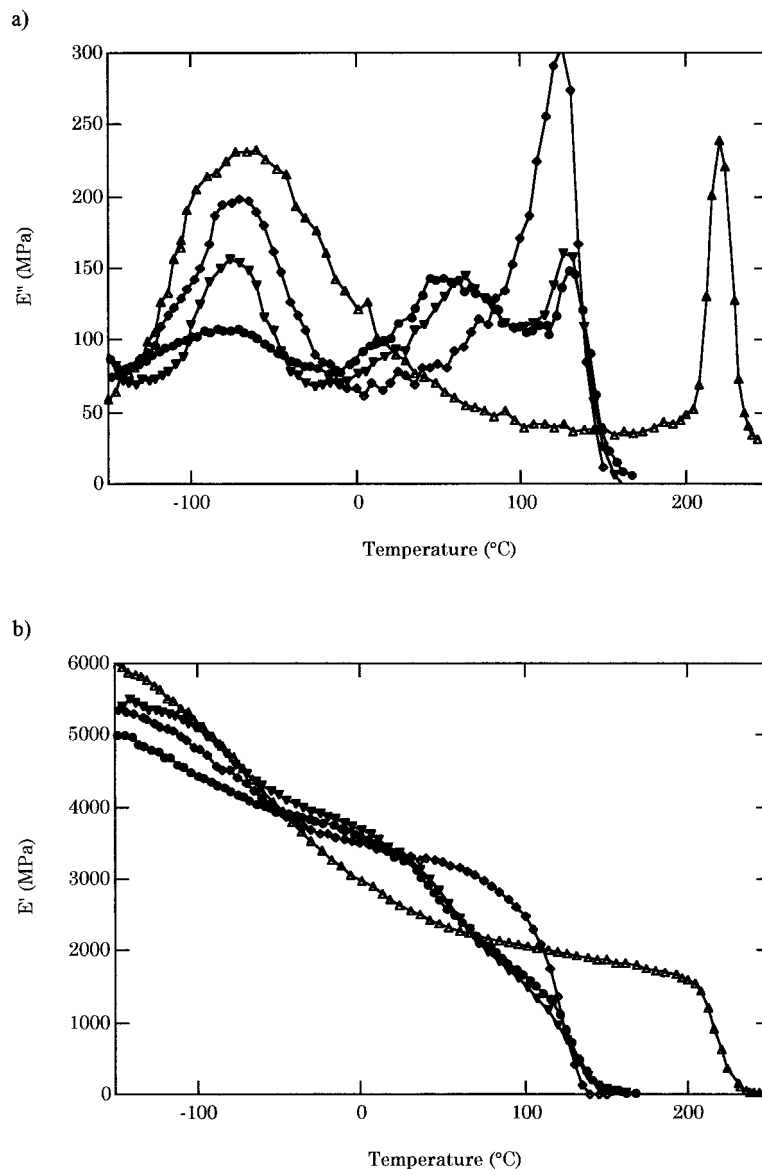
a)

b)

Figure 4 Temperature dependence of the loss and storage moduli at 1 Hz for the samples (△) A–S, (◇) A–S–AA/62, (▼) A–S–AM/62, and (●) A–S–AO/62: (plot a) loss modulus; (plot b) storage modulus.

by eye, of the E'' traces relative to the additives AM and AO shows rather a lowering of the peak amplitude. However, careful analysis also reveals depression of the values of $T\beta(1$ Hz), as can be seen in the first entry of Table V. Thus, all these observations can be justified by the hindrance of the cooperative motions of the chains, as the result of the immobilization of the crosslinks by the additive. In this respect, indeed, the nature of the motions to be hindered (motions of the propyl ether units) is the same for all the systems and, in addition, the general shape and size of the additives are the same.

Further arguments supporting this interpretation can be provided by checking the cooperative character of the motions through the Stark-weather analysis of the activation energies, calculated from measurements at different frequencies [see eqs. (1) and (2)]. Starkweather's model recently proved to be a very useful tool in studies on epoxies[2,9] and also on thermoplastics.[13] As shown in Table V, quite high values of the activation entropy $\Delta S^{\ddagger}$ at the maximum of the β-relaxation are only observed in the case of the pure network A–M and A–S, for which cooperative motions are expected. On the other hand, values of

Table V   Network Characteristics Associated with the β-Relaxation

Code Name	$T\beta(1\text{ Hz})$ (°C)	Ea (kJ mol^{-1})	$\Delta H^{\ddagger}$ (kJ mol^{-1})	$\Delta S^{\ddagger}$ (J K^{-1} mol^{-1})	E' (1 Hz, 25°C) (MPa)
A–M	−70	63	62	80	2700
A–M–AA/29	−72				3300
A–M–AA/62	−83	51	49	44	3800
A–M–AA/96	−88				3900
A–M–AM/29	−76				3000
A–M–AM/62	−83	51	49	33	3400
A–M–AM/96	−95				3500
A–M–AO/62	−82	53	51	33	3400
A–M–AO/96	−90				3000
A–S	−62	71	70	105	2700
A–S–AA/29	−72				3000
A–S–AA/62	−77	53	51	43	3400
A–S–AA/96	−90				3800
A–S–AM/62	−73	56	55	44	3400
A–S–AM/96	−90				3400
A–S–AO/62	−80	49	48	30	3300

$\Delta S^{\ddagger}$ around 40 J K^{-1} mol^{-1} or less are determined in the presence of any of the three additives, as a proof of their antiplasticizing effect. In agreement with a previous report,[14] the efficiency of the antiplasticization in the resins A–M and A–S increases continuously with an increasing amount of additive AA up to 0.96 mol per 4 hydroxypropylether units. This result is no longer verified with the additives AM and AO, for which an optimum is often reached at only 0.62 mol of additive per network repeat unit. This observation will be interpreted later on in this article.

It is important for the applications to pay attention also to the values of the Young's modulus at ambient temperature. Data grouped in the last entry of Table V confirm that the fortifying effect of the additive on the modulus increases as its antiplasticizing effect. The cases for which the increase in the additive amount is not accompanied by an increase in modulus (A–M–AO/96 and A–S–AM/96 for instance) coincide with the saturation of the antiplasticization, as mentioned above.

Analysis of the α-Relaxation for the Systems Formulated with the Additive AA

As can be seen in Figures 3(a) and 4(a), the high-temperature damping peak relative to the networks prepared in the presence of the additive AA may be regarded as pure, at least as a first approximation. This observation validates the idea of a miscibility between the additive AA and the chains of the networks A–M and A–S, as predicted by the values of the solubility parameters (Table III) and corroborated by NMR experiments.[6] As the temperature, $T\alpha$, of the maximum of the E'' peak is systematically located between the pure network glass transition temperature, $T_{g_{\text{pol}}}$, and the additive glass transition temperature, $T_{g_{\text{add}}}$, it is reasonable to assume that the α motions are plasticized by the additive. If the measurements were based on DSC experiments, one could try to account for the dependence of T_g as a function of the weight fraction of the additive, w_{add}, using the Karasz equation, relative to a binary mixture of polymer and diluter[15,16]:

$$T_g = \frac{(1 - w_{\text{add}})\Delta Cp_{\text{pol}}T_{g_{\text{pol}}} + w_{\text{add}}\Delta Cp_{\text{add}}T_{g_{\text{add}}}}{(1 - w_{\text{add}})\Delta Cp_{\text{pol}} + w_{\text{add}}\Delta Cp_{\text{add}}} \quad (11)$$

In our studies, $T\alpha$ values proved to be more reproducible than were T_g values for the pure and plasticized networks. Therefore, calculations were performed by using the "hybrid" equation

$$T\alpha(1\text{ Hz})$$
$$= \frac{(1 - w_{\text{add}})\Delta Cp_{\text{pol}}T\alpha(1\text{ Hz})_{\text{pol}} + w_{\text{add}}\Delta Cp_{\text{add}}T_{g_{\text{add}}}}{(1 - w_{\text{add}})\Delta Cp_{\text{pol}} + w_{\text{add}}\Delta Cp_{\text{add}}}$$
$$(12)$$

The values of $T\alpha(1\text{ Hz})_{\text{pol}}$, $T_{g_{\text{add}}}$, ΔCp_{pol}, and ΔCp_{add} were taken from Table VI. A good agree-

Table VI Characteristics of the Pure Chemicals Used for the Calculations Based on the Karasz Equation

Code Name	T_g (DSC) (°C)	$\Delta Cp(T_g)$ (J g^{-1} K^{-1})	$T\alpha$(1 Hz) (°C)
AA	−14	0.67 ± 0.03	
AM	−23	0.76 ± 0.03	
AO	−45	0.71 ± 0.03	
A–M		0.23 ± 0.03	186
A–S		0.21 ± 0.03	220

ment was found between the experimental and calculated values of $T\alpha$(1 Hz) for any network and w_{add} (Table VII), provided that we adopted for the ΔCp's the values 0.67, 0.23, and 0.20 J K^{-1} g^{-1} for AA, A–M, and A–S, respectively.

This interpretation of the results depends on the epoxy having the same degree of crosslinking. The fact that the Karasz equation is nicely obeyed by the samples A–M–AA and A–S–AA supports the idea that the members of a given series present the same degree of reaction, irrespective of their additive amount. If not, differences of the reaction degree should affect the values of $T\alpha$ and, in turn, should induce substantial data scattering (which is not observed).

Analysis of the α- and μ-Relaxations for the Systems Formulated with the Additives AM and AO

The occurrence of phase separation, anticipated by the solubility parameters (Table III) and clearly confirmed by the NMR experiments,[6] is responsible for the observation of two mechanically active relaxations, μ and α, in the high-temperature range. It is not questionable that glass transition motions of polymer bonds included in the polymer-rich phase are responsible for the α relaxation. Therefore, simple manipulation of eq. (12) permits calculation of the weight fraction of the additive in the phase α, $w_{add}\alpha$, by the equation

$$w_{add}\alpha = \frac{\Delta Cp_{pol}[T\alpha(1\ Hz)_{pol} - T\alpha(1\ Hz)]}{T\alpha(1\ Hz)[\Delta Cp_{add} - \Delta Cp_{pol}] + T\alpha(1\ Hz)_{pol}\Delta Cp_{pol} - T_{g_{add}}\Delta Cp_{add}}$$

(13)

The values of $w_{add}\alpha$ given in Table VIII were calculated using the experimental values of $T\alpha$(1 Hz) (also Table VIII), $T\alpha$(1 Hz)$_{pol}$, and $T_{g_{add}}$ (Table

VI) and adopting for the ΔCp's the values 0.76 and 0.71 J K^{-1} g^{-1} for AM and AO, respectively, and again 0.23 and 0.20 J K^{-1} g^{-1} for A–M and A–S, respectively. As expected, the calculated values of $w_{add}\alpha$ are slightly lower than are the nominal compositions, w_{add}, of the systems (Table IV) and the gap increases with an increasing additive amount.

More interesting is to focus on the characteristics associated with the relaxation μ. First, the frequency dependence of this relaxation can be described by confidence by an Arrhenius plot. However, high values of the activation energy, typically around 250 kJ mol^{-1}, are obtained (Table IX). In addition, Starkweather analysis of these data leads to extremely large values of the activation entropy, typically around 500 J K^{-1} mol^{-1} (Table IX). According to this model, this means that the relaxation μ is highly cooperative. As a consequence, it is reasonable, meaning that glass transition motions are concerned there, in spite of the observed Arrhenius behavior. The normal WLF behavior of such a transition is probably masked here by the restricted range of frequencies available (between 0.05 and 60 Hz). With this assumption, the weight fraction of the additive in the phase μ, $w_{add}\mu$, can be calculated as above by using the equation

$$w_{add}\mu = \frac{\Delta Cp_{pol}[T\alpha(1\ Hz)_{pol} - T\mu(1\ Hz)]}{T\mu(1\ Hz)[\Delta Cp_{add} - \Delta Cp_{pol}] + T\alpha(1\ Hz)_{pol}\Delta Cp_{pol} - T_{g_{add}}\Delta Cp_{add}}$$

(14)

The values of $w_{add}\mu$ thus obtained (Table VIII) show that the amount of the additive present in the phase μ, although much larger than the nominal composition of the system, is small, especially at a low nominal amount w_{add}. It is easy to cal-

Table VII Comparison of Experimental and Calculated Values of $T\alpha$(1 Hz) for the Resins Formulated with the Additive AA

Code Name	$T\alpha$(1 Hz) (°C), Measured	$T\alpha$(1 Hz) (°C), Calculated
A–M–AA/29	138	141
A–M–AA/62	106	110
A–M–AA/96	90	88
A–S–AA/29	167	163
A–S–AA/62	125	126
A–S–AA/96	102	101

Table VIII   Calculation of the Weight Fraction of Additives in the Phases α and μ and of the Weight Fraction of Phase μ for the Resins Formulated with the Additives AM and AO

Code Name	$T\alpha(1\ Hz)\ (°C)$ Measured	$T\mu(1\ Hz)\ (°C)$ Measured	$w_{add}\alpha$ Calculated	$w_{add}\mu$ Calculated	$w_{phase\ \mu}$ Calculated
A–M–AM/29	143	86	0.0738	0.2216	0.0419
A–M–AM/62	114	65	0.1396	0.3004	0.0896
A–M–AM/96	96	44	0.1898	0.4007	0.1432
A–M–AO/62	110	50	0.1371	0.3168	0.1330
A–M–AO/96	87	35	0.1955	0.3794	0.1570
A–S–AM/62	130	63	0.1340	0.3245	0.0682
A–S–AM/96	105	50	0.1912	0.3800	0.1049
A–S–AO/62	130	53	0.1265	0.3243	0.1391

The four figures appearing for the values of $w_{add}\alpha$, $w_{add}\mu$, and $w_{phase\ \mu}$ are not significant. They are just given to permit a check of their calculation from the values of $T\alpha$ and $T\mu$ by using the eqs. (13)–(15).

culate from Table VIII that, at the outmost, there is, on average, 0.4 mol of additive molecule per hydroxypropyl ether unit of the epoxy chain.

It is worth noting that large uncertainties may affect the values of $w_{add}\alpha$ and $w_{add}\mu$. Indeed, small changes on the experimental evaluations of $T\alpha(1\ Hz)$ and $T\mu(1\ Hz)$ are likely to cause substantial changes of the values of $w_{add}\alpha$ and, especially, $w_{add}\mu$. As a consequence, it is impossible to comment on the influence of the chemical structure of both the additive and the network. By contrast, the results show clearly (Fig. 5) the effect of the amount of the additive on phase compositions. A crude estimate of the weight fraction of phase μ in the material, $w_{phase\ \mu}$, can be made from these data just by applying the principle of mass conservation to the two components of the two-phase system. It turns out that

$$w_{phase\ \mu} = \frac{w_{add} - w_{add}\alpha}{w_{add}\mu - w_{add}\alpha} \qquad (15)$$

The calculated values of $w_{phase\ \mu}$ are given in the last entry of Table VIII. Even if these calculations

may be regarded with a certain reservation, they show, unambiguously, that the overall extent of the phase μ is quite small in the materials under study.

Summing up the information collected in this section about the relaxations β, μ, and α, the following picture of the phase separation observed in the networks formulated with the antiplasticizers AM and AO can be proposed. The domains occupied by the phase α, strongly predominant in the materials, consist of polymer segments in interaction with a slightly lower number of additive molecules than that encountered for the systems formulated with the additive AA. The other additive molecules, which are rejected out of the phase α during the network formation, are also of a minority in the phase μ. Therefore, if it is still understandable that part of the additive molecules may interact with each other inside the μ phase, one does bear in mind that the μ domains are chemically linked to the α domains by means of crosslinked polymer chains. Anyway, the average number of additive molecules per hydroxypropyl ether unit of the networks is probably too

Table IX   Characteristic Temperature, $T\mu$, and Activation Energy, Ea, Enthalpy, $\Delta H^{\ddagger}$, and Entropy, $\Delta S^{\ddagger}$, at the Maximum of the μ-Relaxation

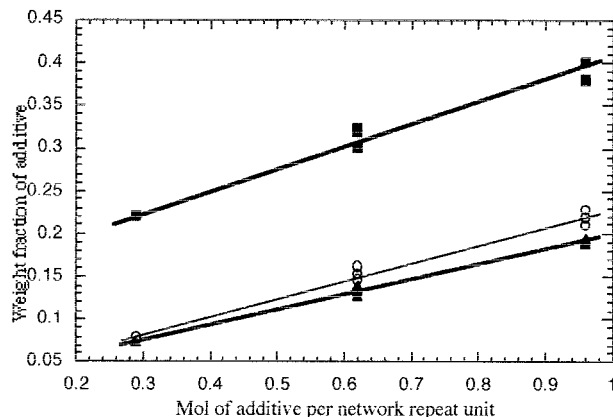| Code Name	$T\mu$ (°C)	Ea (kJ mol^{-1})	$\Delta H^{\ddagger}$ (kJ mol^{-1})	$\Delta S^{\ddagger}$ (J K^{-1} mol^{-1})
A–M–AM/62	61	275	270	580
A–M–AO/62	50	255	250	550
A–S–AM/62	56	240	235	500
A–S–AO/62	45	235	230	480

Figure 5 Additive weight fraction versus mol number of additive per network repeat unit. (○) Nominal weight fraction in the material; (▲) calculated weight fraction in phase α; (■) calculated weight fraction in phase μ.

large with respect to the antiplasticization phenomenon. This is the reason why some saturation of this effect is observed. In addition, one may suggest that the μ domains, which represent a small proportion of the overall materials are of nanometric size, in agreement with the fact that they are not detected, for instance, by electron microscopy and that they just show up at the spatial scale of the NMR experiments.[6]

Analysis of the Fracture Behavior

Because fracture experiments are very much time- and chemical-consuming, measurements were performed on a restricted number of systems. The resin A–S–AM/62 was selected, as representative of the overall study on biphasic materials and as a realistic candidate for potential applications. The resins A–S and A–S–AA/62 were also investigated, for the sake of comparison. Experiments were performed over the temperature range −20/80°C, which is interesting for the applications.

Type of Rupture

According to the shape of the load-displacement curves (Fig. 6), two types of fracture behavior can be identified on the reference samples A–S. In stable rupture conditions (so-called type C rupture), the load first increases linearly until a maximum value and then decreases slowly to zero: The area under the increasing part of the loading curve defines the energy necessary for crack initiation, whereas the area under the decreasing

part of the curve corresponds to the energy necessary for crack propagation. In unstable rupture conditions (type B rupture), the linear loading step is followed by an abrupt drop to zero, as the result of instantaneous crack propagation in the sample. The former situation is encountered with A–S for tests carried out at room temperature [Fig. 6(a)], whereas the latter is observed at higher temperature [Fig. 6(b)]. These observations are consistent with the earlier conclusions of Kinloch et al.[17] According to these authors, the fracture behavior of resins at a given displacement rate is highly sensitive to temperature. It moves from being fragile stable (type C) at low temperature to fragile unstable (type B) at higher temperature, before reaching a ductile stable crack growth (type A) at temperatures close to the T_g. As A–S presents a particularly high $T\alpha$ value (Table VI), ductile behavior could not be observed
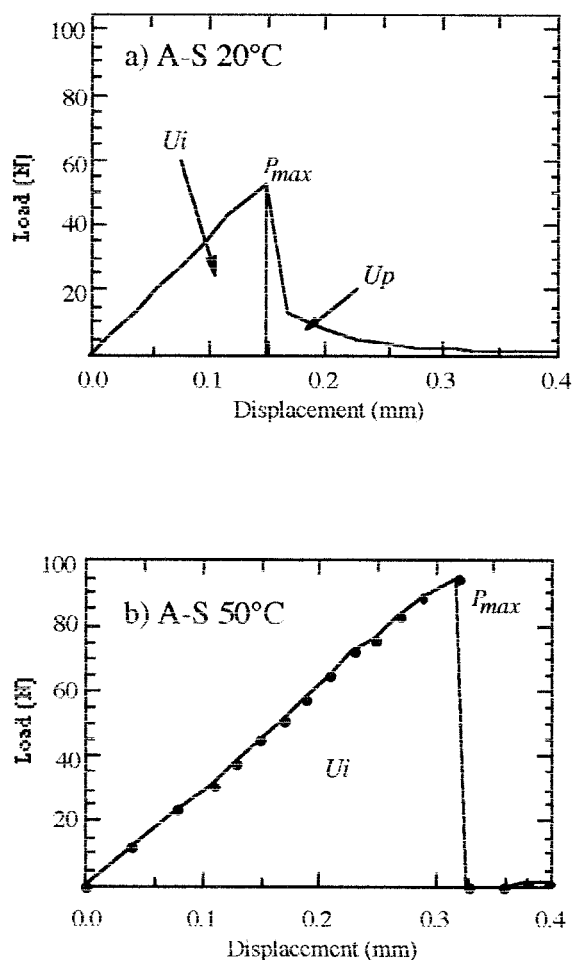

Figure 6 Typical plots of load versus displacement for the sample A–S in three-point bending geometry at a crosshead speed of 1 mm mn^{-1}. (Plot a) Stable rupture at 20°C; (plot b) unstable rupture at 50°C.
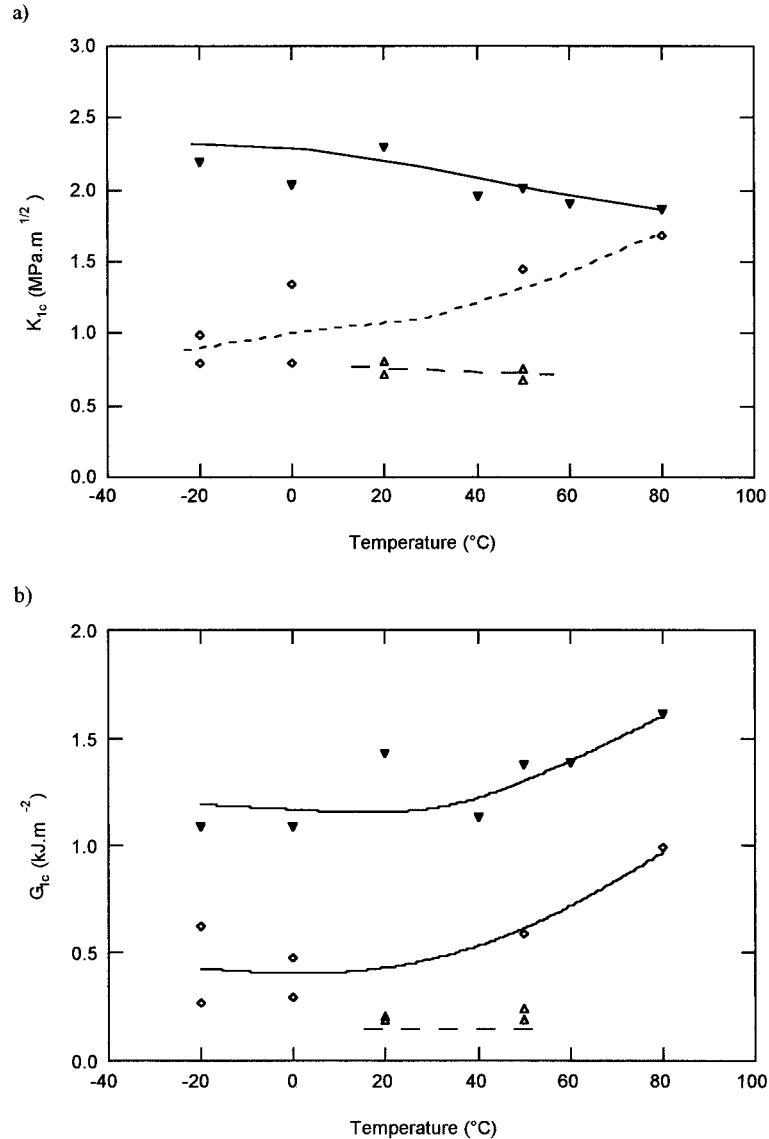
a)

b)

Figure 7 Temperature dependence of K_{Ic} and G_{Ic} for the samples ($\triangle$) A–S, ($\diamond$) A–S–AA/62, and ($\blacktriangledown$) A–S–AM/62. (Plot a) K_{Ic}; (plot b) G_{Ic}.

at 80°C and the transition from type C to type B rupture occurred around room temperature.

Study of the fracture behavior of the resins A–S formulated with AA and AM additives revealed systematically the occurrence of fragile unstable rupture (type B) all over the range −20/80°C (data not shown). Probably, the depression of $T\alpha$ in the antiplasticized resins (Table V) induces a shift of the type C/type B transition down to temperatures lower than −20°C. In addition, no ductile behavior is observed at 80°C.

K_{Ic} and G_{Ic} Values

Plots of K_{Ic} and G_{Ic} as a function of the test temperature are, respectively, shown in Figure

7(a,b) for the neat and modified resins A–S. As expected, both quantities present the same type of temperature dependence. The pure resin A–S exhibits relatively low tenacity values, reflecting the well-known poor crack resistance of highly crosslinked epoxy materials at temperatures well below their T_g. In comparison, the antiplasticized resin A–S–AA/62 behaves the same below or around room temperature and then presents a moderate increase in tenacity at the approach of T_g. By contrast, the resin A–S–AM/62 presents much greater tenacity over the entire temperature range studied. Besides, the toughness enhancement occurs even at −20°C, although the μ phase is probably glassy at the characteristic time
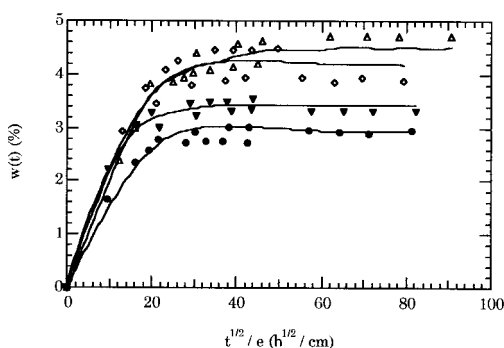
a)
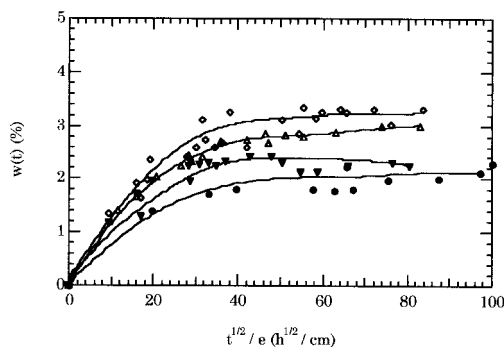
b)

Figure 8   Kinetics of water uptake at 100°C for pure and formulated networks: (plot a) (△) A–M, (◇) A–M–AA/62, (▼) A–M–AM/62, (●) A–M–AO/62; (plot b) (△) A–S, (◇) A–S–AA/62, (▼) A–S–AM/62, (●) A–S–AO/62.

scale of the test, defined by the velocity of crack propagation through the material. Differences in the temperature dependence of the Young's modulus and yield stress of the different samples may be invoked to justify the toughening at high temperature[5,14] of the antiplasticized samples A–S–AA/62 and A–S–AM/62. On the other hand, these arguments do not hold to explain the peculiar behavior of the sample A–S–AM/62 between −20 and 40°C, a temperature range where the three samples present almost the same yield stress values.

Actually, the strong toughening effect observed over a broad temperature range in the AM formulation is assigned to its very special morphology, as discussed above. A realistic mechanism might involve a stress concentration localized in the μ domains, able to favor plastic flow in the matrix, in agreement with the toughening mechanism involved in rubber-modified epoxy systems. However, because the network spreads over the entire resin volume, localized cavitation at the aggregate/matrix interface cannot exist and, therefore, a possible deformation process might be shear yielding. This idea is corroborated by the absence of any stress-whitening effect in the sample A–S–AM/62.

Sensitivity of the Networks to Water Uptake

It is well known that an excessive water uptake is detrimental to many applications of the epoxies. As a consequence, it was important, in the last step of this study, to determine whether the novel formulations leading to improved toughening are less (more) sensitive to moisture than are the pure resins. To answer this question and also to understand the mechanism of water diffusion in the resins, experiments were carried out on most of the samples given in Table IV. Figure 8 shows some examples of the observed temperature dependence of $w(t)$. Drawings were made by plotting $w(t)$ versus $t_{1/2}/e$ with the aim of (1) accounting for the measurements at different sample thickness e, (2) determining easily the water uptake at equilibrium w_∞, and (3) checking the short-term Fickian behavior.

Table X   Water-uptake Characteristics

Code Name	Water Uptake at Equilibrium, w_∞ (%)	Fickian Diffusion Coefficient, D (cm^2 s^{-1})
A–M	3.0 ± 0.2	$(0.7 \pm 0.2) \times 10^{-7}$
A–M–AA/29	2.5	0.6×10^{-7}
A–M–AA/62	3.3	0.7×10^{-7}
A–M–AA/96	3.5	0.7×10^{-7}
A–M–AM/62	2.3	0.8×10^{-7}
A–M–AM/96	2.2	0.7×10^{-7}
A–M–AO/62	2.1	0.7×10^{-7}
A–M–AO/96	2.4	0.8×10^{-7}
A–S	4.5 ± 0.2	$(1.1 \pm 0.3) \times 10^{-7}$
A–S–AA/29	3.8	1.3×10^{-7}
A–S–AA/62	4.2	1.6×10^{-7}
A–S–AA/96	4.5	2.4×10^{-7}
A–S–AM/62	3.4	2.2×10^{-7}
A–S–AM/96	3.0	1.8×10^{-7}
A–S–AO/62	3.0	1.5×10^{-7}

Water Uptake at Equilibrium

Values of w_∞ are presented in Table X. Comparison of the data relative to the samples A–M and A–S, which present roughly the same crosslink density, highlights the influence of the polarity of the medium. Because DDS, which contains a sulfone moiety, is more polar than is DDM, then w_∞ is larger for A–S than for A–M. As a first approximation, formulation of both materials with the compatible additive AA (of solubility parameter and polarity comparable to those of the pure matrices) does not change markedly the values of w_∞, whatever the amount of additive. By contrast, use of the additives AM and AO leads, in each case, to a substantial reduction of the values of w_∞, which are, again, weakly influenced by the amount of the additive. As recalled in a recent article by Soles et al.,[18] this effect is likely to be provoked by decrease of the additive polarity and (or) by modification of the chain topology. It seems that the former effect prevails, as w_∞ decreases from AM to AO (less polar, because of the absence of OH functions) and that it is not markedly affected by changes in the additive amount, that is, by changes in the morphology of the biphasic structure.

Fickian Diffusion Coefficient

Table X also gives the values of the diffusion coefficient D, calculated by using eq. (10). Systematically, samples of the series A–S present larger values of D than those of the series A–M. In pure

networks, D has been shown, on the contrary to w_∞, to be strongly influenced by the network architecture.[19,20] At given chemical structure, loosely crosslinked networks absorb water much more slowly than do the densely crosslinked ones. This result was explained by considering that the kinetics of water diffusion is controlled by the β-relaxation motions: The more numerous they are, the larger the diffusion coefficient.

As it is apparent from the comparison of Figures 3(a) and 4(a) that the β-relaxation is broader for A–S than for A–M, then the above analysis contributes to explain why D is larger for pure A–S than for pure A–M. An additional argument comes from the increase in polarity from A–M to A–S, which also favors water diffusion.

No significant difference shows up between the values of D, while comparing the samples A–M and A–M–additive. Therefore, the expected decrease of the diffusion coefficient resulting from the antiplasticization is balanced in these cases by the antagonist effects either of the polar additive AA or of the biphasic morphology (additives AM and AO). In the case of the samples A–S and A–S–additive, it turns out that the latter effects prevail on the former. However, D tends to decrease, as expected, while suppressing any hydrogen bonding from the additive AO.

CONCLUSIONS

The interest provided by the addition of an antiplasticizing agent in the formulation of epoxy–

amine resins is strongly enhanced by selecting, as the antiplasticizer, a chemical species which is fully miscible with the mixture of monomers but gives rise to nanoscale phase separation along the network construction. The networks prepared in this way are shown (1) to save a sufficiently high value of T_g in the view of the applications, (2) to present a higher modulus and higher toughness around room temperature than those of the conventional systems without an additive, and (3) to exhibit a lower water uptake at equilibrium than that of their regular homologs. In addition, these novel formulations offer a double interest for potential industrial applications: First, they are based on additives which can be easily synthesized, and, second, they use the same cure cycle as that commonly adopted for the preparation of the regular pure resins.

REFERENCES

1. Daly, J.; Britten, A.; Garton, A. J Appl Polym Sci 1984, 29, 1403.
2. Heux, L.; Lauprêtre, F.; Halary, J. L.; Monnerie, L. Polymer 1998, 39, 1269.
3. Merritt, M. E.; Goetz, J. M.; Whitney, D.; Chang, C. P.; Heux, L.; Halary, J. L.; Schaefer, J. Macromolecules 1998, 31, 1214.
4. Barton, A. F. M. Handbook of Solubility Parameters, 2nd ed.; CRC: Boca Raton, FL, 1991.
5. Sauvant, V. Thesis, University P. M. Curie, Paris, 1999.
6. Sauvant, V.; Lauprêtre, F., submitted for publication in Polymer.
7. Girard-Reydet, E.; Riccardi, C. C.; Sautereau, H.; Pascault, J. P. Macromolecules 1995, 28, 7599.
8. Barrère-Tricca, C. Thesis, University P. M. Curie, Paris, 1998.
9. Heux, L.; Halary, J. L.; Lauprêtre, F.; Monnerie, L. Polymer 1997, 38, 1767.
10. Starkweather, H. W. J. Macromolecules 1981, 14, 1277.
11. Williams, J. G., In A Linear Elastic Fracture Mechanics Standard for Determining K_c and G_c for Plastics; EGF Task Group on Polymers and Composites: London, 1989.
12. Crank, J. The Mathematic of Diffusion; Clarendon: Oxford, 1956.
13. Beaume, F.; Brulé, B.; Halary, J. L.; Lauprêtre, F.; Monnerie, L. Polymer 2000, 41, 5451.
14. Halary, J. L.; Heux, L.; Rana, D.; Sauvant, V.; Monnerie, L. Proc Am Chem Soc Div PMSE 1996, 75, 358.
15. Ten Brinke, G.; Karasz, F. E.; Ellis, T. S. Macromolecules 1983, 16, 244.
16. Ellis, T. S.; Karasz, F. E.; Ten Brinke, G. J Appl Polym Sci 1983, 28, 23.
17. Kinloch, A. J.; Shaws, S. J.; Todd, D. A.; Hunston, D. L. Polymer 1983, 24, 1341.
18. Soles, C. L.; Chang, F. T.; Bolan, B. A.; Hristov, H. A.; Gidley, D. W.; Yee, A. F. J Polym Sci Part B Polym Phys 1998, 36, 3035.
19. Halary, J. L.; Cukierman, S.; Monnerie, L. Ann Compos 1992, 1–2, 103.
20. Halary, J. L. High Perform Polym 2000, 12, 141.